



Anisotropic plasticity deformation during micro-deep drawing of 304 foils: An experimental and numerical investigation

Lei Shang^{1,2} · Suxia Huang^{1,3} · Jianhua Hu^{1,2} · Hezong Li^{1,2}  · Yong Pang⁴

Received: 24 September 2023 / Accepted: 28 February 2024 / Published online: 15 March 2024
© The Author(s), under exclusive licence to Springer-Verlag France SAS, part of Springer Nature 2024

Abstract

The purpose of this work is to study the effect of anisotropic plasticity on the micro-deep drawing of the 304 stainless steel foils through a combination of experimental testing and numerical modeling. A phenomenological anisotropic model, with the Yld2004-18p yield function, is used to model the anisotropic plasticity deformation of the material. Based on the miniature tensile experimental data and Voce's hardening law, the coefficients in the Yld2004-18p function were calibrated. The FE modelling was implemented using ABAQUS to simulate the micro-deep drawing experiments. The wall thickness and height of the cylindrical cup obtained by the simulation have shown to be reasonably close to the experimental values, and the distribution of ears is the same as the experimental results. It has shown that the Yld2004-18p anisotropic yield function can accurately describe the anisotropic behavior of 304 stainless steel foils during the micro-deep drawing process.

Keywords 304 stainless steels foils · Anisotropic plasticity · Yld2004-18p yield function · Micro-deep drawing · Finite element modelling

Introduction

Driven by the continuous miniaturization of communication [1], micro-electromechanical systems [2], optics [3], medical [4], transportation [5] and other fields, the demand for micro metal parts has increased rapidly. However, products manufactured by micro-forming processes are affected by many factors, such as anisotropy and size effects of the forming material. As a major micro-forming process, micro-drawing has been widely used in forming hollow, thin-walled, cylindrical and other micro-metal parts. Therefore, the study of

material anisotropy is significant in improving the quality of micro-forming products.

The quality of micro-deep drawing products is significantly affected by material properties [6]. Shimizu et al. [6] studied the influence of anisotropic properties on the formability of bronze foil in micro-deep drawing experiments and found that the formability of bronze foil is affected by both geometric anisotropy and material anisotropy. Tang et al. [7] carried out deep drawing tests on cross rolling and unidirectional rolling plates and obtained higher anisotropy value Δr (value of planar anisotropy) and larger elongation, which can obtain cylindrical cups with higher depth. Deminet et al. [8] proposed a mathematical model that can predict the ears height and its dependence on the anisotropy value Δr and the drawing ratio and determined the maximum drawing ratio and anisotropy coefficient for drawing. Yoon et al. [9] studied the influence of anisotropic evolution on the prediction of ears in cylindrical cups. They used two anisotropic yield functions (Yld2000-2d and Cazacu-Plunkett-Barlat [10]) to define the anisotropic yielding behaviour of AA5042-H2 thin plate materials. They expressed the coefficients of these yield criteria as functions of equivalent plastic strain. It is pointed out that the Cazacu-Plunkett-Barlat criterion based on plastic strain can predict the shape and height of a cylindrical cup. Dorel Banabic [11] innovatively derived

✉ Hezong Li
lhong@hebeu.edu.cn

✉ Yong Pang
yong.pang@qmul.ac.uk

¹ School of Mechanical and Equipment Engineering, Hebei University of Engineering, Handan 056038, China

² Key Laboratory of Intelligent Industrial Equipment Technology of Hebei Province, Handan 056038, China

³ School of Mechanical Engineering, University of Science and Technology Beijing, Beijing 100083, China

⁴ School of Engineering and Materials Science, Queen Mary University of London, London WC1E 7HU, UK

a more general and accurate anisotropic yield criterion and established a metal material model considering anisotropy and hardening effects. The established anisotropic yield criterion and material model can accurately describe the mechanical behavior of anisotropic materials, which provides an important reference for numerical simulation and engineering application in metal forming. Anne Marie Habraken et al. [12] is based on the finite element simulation of AA6016-T4 aluminum alloy cup deep drawing process in ESAFORM 2021 benchmark test. Different parameter identification methods (relying on physical test data, combined with virtual test data, etc.) are used for model calibration. By combining the physical test data and the virtual test data for parameter identification, the accuracy of the simulation results is improved. Lou [13] introduced the simplified Yld2004-18p function to simulate the stamping process of aluminium alloy and used the virtual model to reproduce the actual stamping process of most aluminium alloys. Rong et al. [14] used the Yld2004-18p function to accurately predict the spatial fluctuation of the convex ear contour in simulation.

During the rolling process, the grains in the material will produce dislocation slip and twin deformation, so the grains will have a preferred orientation arrangement, which is manifested as the anisotropy of mechanical properties at the macro level [15–18]. Moreover, because the deep drawing theory based on the cylindrical cup is based on the assumption of material isotropy, the influence of sheet anisotropy on the deep drawing performance of cylindrical deep drawing parts, such as stress-strain distribution, cylinder wall thickness and ear phenomenon, cannot be shown [19–21].

The anisotropy of the metal sheet will cause the forming defect of ears of the cylindrical cup induced by drawing. Accurate prediction of the ears phenomenon of the cylindrical cup is essential for manufacturing. In this work, the 304 stainless steel foils are used as raw material to carry out uniaxial tensile test and micro-deep drawing test. The influence of orientation on the tensile results is revealed, and the influence of sheet thickness and punch diameter on deep drawing is evaluated.

After that, the Yld2004-18p, yield function is introduced to simulate the micro-deep drawing process and the appearance of the cylindrical cup, and the stage division and stress-strain analysis of each part of the 304 stainless steel sheet deep drawing process are innovatively carried out. The purpose is to accurately simulate the anisotropic behavior of the deep drawing process by finite element method, so as to more accurately simulate the deformation process of the

cylindrical cup under complex stress state. This will help to optimise the shape design of the cylindrical cups and determine the process parameters. The developed, experimentally validated numerical modelling methodology can provide a holistic and effective tool, with the predictive capability to study the role of plasticity anisotropy, and to determine plastic forming configurations, which are critically important for ultra-thin sheet forming design, manufacturing, and evaluation. In addition, the current model also has the potential to be extended to study the intrinsic and extrinsic size effects on the micro-deep drawing forming process.

Experiment work

The 304 stainless steel foils

The 304 stainless steel foils are made by cold rolling with a thickness of 100 μm . The chemical composition is shown in Table 1. To determine the influence of anisotropy on the mechanical properties, the miniature tensile specimens were cut from a rolling direction (0°) to a transverse direction (90°) at an increment of 15° using wire electrical discharge machining. For special materials that are difficult or expensive to obtain, small size specimens provide the possibility to increase test options and obtain more test data. Considering the convenience of sampling and the effective reduction of test cost, it is of great theoretical significance and engineering application value to realize the research on the material and equipment performance of small size samples. The dimensions of the specimen are designed according to the principle of similar reduction to the standard uniaxial tensile specimen, as shown in Fig. 1. After the sample processing is completed, the oil stain on the surface of the sample is washed with anhydrous ethanol. The gauge section of the sample was finely ground with sandpaper and the sample was preserved in isolated air.

The micro-deep drawing experiment

The micro deep drawing test system comprises a deep drawing die with high matching accuracy and a CMT4000 series electronic universal testing machine, which can automatically control the load and displacement with high precision and constant speed. The maximum test force of the equipment used in this test is 20 KN, the relative error of force control rate is within 0.1 %, the displacement resolution is 0.03 μm , and the maximum forming rate is 500 mm/min,

Table 1 Chemical composition of stainless steel foils

Composition	C	Mn	S	P	Si	Cr	Ni
Content(%)	0.05	0.97	0.007	0.028	0.6	16.59	8.75

which meets the test requirements and ensures the smooth progress of the test.

It can be seen from Fig. 2 that the upper template and the lower template fix the punch and the die, and the electronic universal testing machine connects the handle of the upper template and the lower template. In the micro-deep drawing test process, the punch fixed on the upper template moves downward. After the punch passes through the blank holder, it contacts the material. Under the pressure of the punch, the material undergoes plastic deformation and eventually reaches the mould cavity. The whole drawing test was completed.

The shape and size of the sheet and the cylindrical cup's appearance and size will affect the micro-deep drawing results. In this drawing test, the sheet's thickness and the punch's diameter are taken as the research objects, and the drawing test of the cylindrical cup of 304 stainless steel foils is carried out. The specific experimental design is shown in Table 2 to obtain the deep drawing results under different experimental conditions.

Among them, t is the thickness of the sheet, D_p and R_p are the diameter of the punch and the radius of the punch fillet, respectively, D_d and R_d are the diameter of the die and the radius of the die fillet, respectively, C is the gap distance

Fig. 1 Dimensions of the miniature tensile specimen (mm)

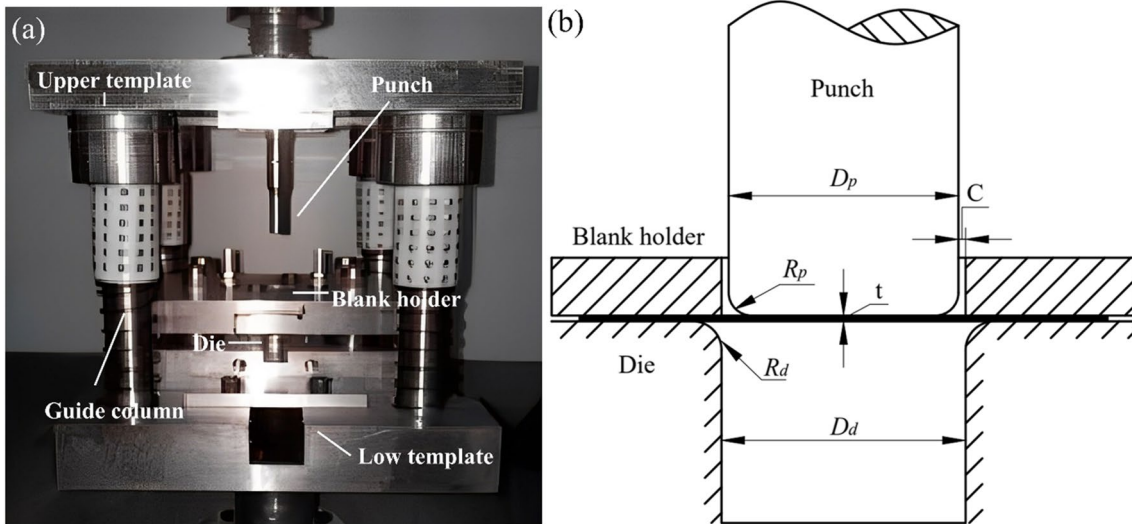
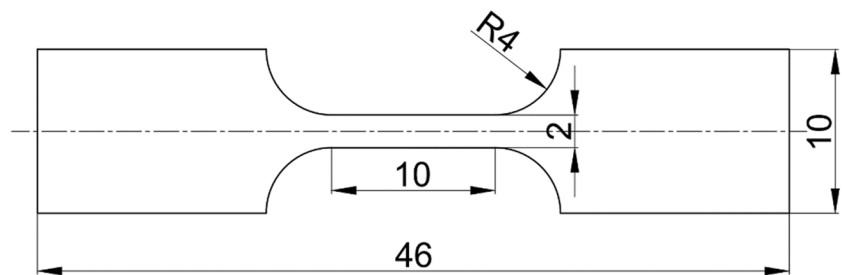


Fig. 2 Micro-deep drawing: (a) the test rig, and (b) a schematic diagram of the punch and support system

Table 2 Design of the micro-deep drawing experiments

Thickness	Punch diameter	Die diameter	Punch radius	Die radius	Clearance	Drawing velocity
t (mm)	D_p (mm)	D_d (mm)	R_p (mm)	R_d (mm)	C (mm)	V (mm/min)
0.05	5	5.125	0.5	0.25	0.0625	1
0.1	5	5.25	0.5	0.5	0.125	2
0.2	5	5.5	0.5	1	0.25	4
0.02	1	1.05	0.1	0.1	0.025	0.4
0.02	2	2.05	0.2	0.1	0.025	0.4
0.02	4	4.05	0.4	0.1	0.025	0.4

between the punch and the die, and V is the drawing speed. Blank holder force can prevent the sample from wrinkling in the process of deep drawing deformation. In the experiment, applying different sizes of blank holder force to different thickness plates is necessary. The empirical formula of blank holder force is as follows:

$$Q = \frac{\pi}{4} (D^2 - (D_d + 2r_d)^2) q \tag{1}$$

where Q is the blank holder force (N), D is the blank diameter (mm); q is the unit blank holder force (MPa). The unit blank holder force of stainless steel is 3MPa ~ 4.5MPa, according to empirical formula, which is 3.75 MPa in this paper.

Deep drawing of cylindrical cups with the same punch diameter at room temperature, in the same drawing ratio (DR), the drawing force-punch stroke curves of different plate thicknesses were analyzed. For the punch diameter of 5mm, the influence of thickness on the drawing force curve is analyzed. The drawing force-punch stroke curves under different thicknesses are as Fig. 3a.

From the curve trend in Fig. 3 and combined with the drawing test process, it can be seen that in stage I of deep drawing, the blank and the punch began to contact, and the drawing force of the sheet with different thicknesses was

not much different. With the increase of the punch stroke, the blank continues to flow into the mould, and the drawing force increases rapidly. The increase rate of drawing force increases with the increase of sample thickness. With the progress of the drawing process, the drawing force of the sheet with a larger thickness increases continuously. In comparison, the increasing rate of the drawing force of the sheet with smaller thickness decreases gradually and finally reaches the maximum drawing force [22]. The displacement of different thickness plates when the drawing force reaches the maximum will increase with the increase of the thickness of the sample. When the punch diameter is constant, the greater the thickness of the sheet, the greater the punch stroke and the greater the drawing force.

At room temperature, under the condition that the thickness of the sheet is 0.02 mm and the same drawing ratio, the drawing test is carried out with the punch diameter of 4mm, 2mm and 1mm, respectively, and the drawing force-stroke curve is shown in Fig. 4a.

Comparing the drawing force-punch stroke curves of cylindrical cup with different punch diameters, combined with the test process, the following conclusions can be drawn: In the stage I of deep drawing, the drawing forces of cylindrical cups with different punch diameters are not much different. After that, with the progress of the experiment,

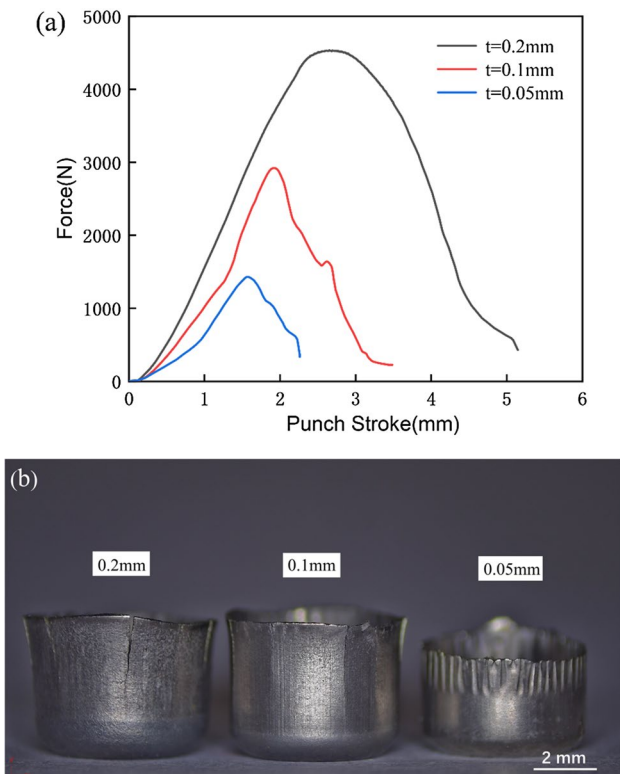


Fig. 3 Micro deep drawing with different thickness of 5mm punch diameter (a) Drawing curves and (b) Formed specimens

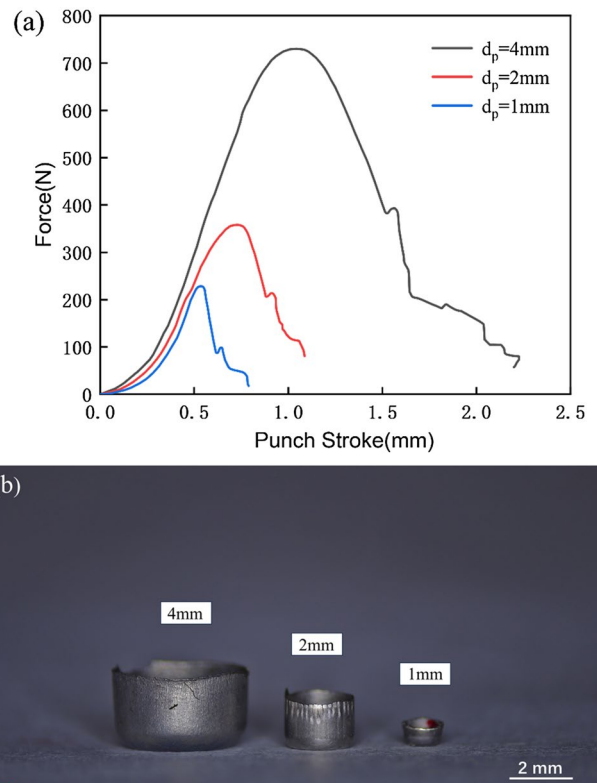


Fig. 4 Micro deep drawing with with different punch diameter of 0.02 mm sheet (a) Drawing curves and (b) Formed specimens

the drawing force increases rapidly with the increase of the punch stroke, and the change rate is roughly the same. With the progress of drawing, the drawing force of cylindrical cups with larger punch diameters is increasing rapidly. After the drawing force reaches the maximum value, the drawing force decreases rapidly until the whole drawing test is completed. For cylindrical cups with different punch diameters, the displacement when the drawing force reaches the maximum value increases with the increase of the diameter of the punch. That is, when the thickness of the sheet is constant, the larger the diameter of the punch is, the greater the drawing force is, and the larger the punch stroke is.

Miniature uniaxial tensile testing

ElectroForce 3200 Series III testing machine is used in the test, as shown in Fig. 5. The maximum load is ± 450 N, and the maximum displacement is ± 6.5 mm. In order to explore the influence of anisotropy, micro-tensile tests were carried out on specimens with a thickness of 0.1 mm and different orientations along the rolling direction at a strain rate of $1 \times 10^{-3} s^{-1}$ at room temperature. In the test, the length direction of the gauge section of the sample is along the direction of the force applied by the test machine, and the geometric centre of the sample is located in the vertical direction of the geometric centre of the fixture. The test machine chuck with thread is used to clamp and fix the sample to ensure test accuracy. During the test, the tensile test under the same conditions was repeated three times.

The true stress-strain curve obtained from the test is shown in Fig. 6. The mechanical properties of the samples at different angles and the standard deviation of the data are shown in Table 3. The tensile curve shows that for the 304 stainless steel sheet prepared by cold rolling, different orientations along the rolling direction can affect the mechanical properties, and the material has anisotropy. When the angle between the sample orientation and the rolling direction increases from 0° to 90° , the yield strength of the sample

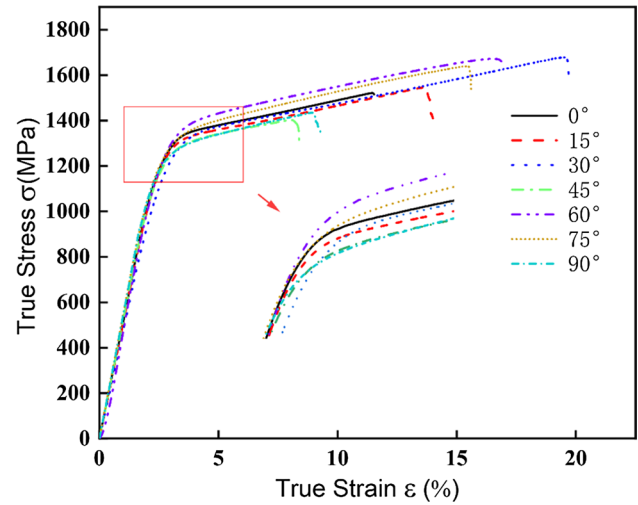


Fig. 6 True stress-strain curves of specimens with different orientations

shows a trend of decreasing first and then increasing, except for 60° . The yield strength value is the smallest when the sample is 45° with the rolling direction. The elongation increases first and then decreases with the angle increase between the sample orientation and the rolling direction. The elongation is the smallest when the sample and the rolling direction are 90° .

Phenomenological anisotropic constitutive model

Phenomenological anisotropic model

The constitutive model of metal's elasto-plasticity consists of three main parts: yield criteria, flow rules, and hardening laws [23]. The flow rule is primarily used to describe the relationship between strain increments and stress. In the constitutive model

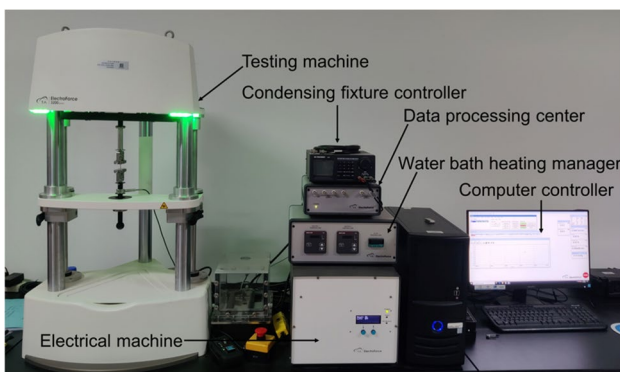


Fig. 5 ElectroForce 3200 Series III testing machine

Table 3 Mechanical properties parameters of specimens with different orientations along the rolling direction

Along the roll- ing direction	Yield strength (MPa)	Standard deviation	Breaking elongation (%)	Standard deviation
0°	1170	10.5	7.59	0.37
15°	1152	4.5	5.77	1.34
30°	1106	29.8	11.74	3.70
45°	1105	26.5	10.76	1.05
60°	1178	4.5	14.97	1.84
75°	1124	52.6	13.62	1.85
90°	1114	5.5	6.36	1.45

describing the plastic deformation of metal, the flow rule represents the direction of deformation during plastic deformation. Based on the relationship between plastic potential and yield function, the flow rule is divided into associated flow rule and non-associated flow rule. The relationship between stress and the rate of plastic strain can be expressed as:

$$\dot{\epsilon} = \dot{\lambda} \frac{\partial \Phi}{\partial \sigma} \tag{2}$$

Where $\dot{\lambda}$ is a non-negative scale factor called the plastic strain multiplier and Φ is the plastic potential function. In order to facilitate the calculation and analysis, this paper selects the associated flow rule.

The Yld2004-18p yield function

The advanced Yld2004-18p yield function is introduced. The constitutive model based on this yield function describes the anisotropic behaviour of 304 stainless steel through the user material subroutine UMAT. The Yld2004-18p anisotropic yield function is one of the most commonly used high-precision non-quadratic yield functions to describe the anisotropic behaviour of BCC materials and FCC materials. The expression is:

$$\begin{aligned} \phi &= \phi(\Sigma) = \phi(\tilde{S}', \tilde{S}'') \\ &= [\tilde{S}'_1 - \tilde{S}''_1]^a + [\tilde{S}'_2 - \tilde{S}''_2]^a + [\tilde{S}'_3 - \tilde{S}''_3]^a + [\tilde{S}'_2 - \tilde{S}''_1]^a + [\tilde{S}'_2 - \tilde{S}''_3]^a \\ &+ [\tilde{S}'_3 - \tilde{S}''_1]^a + [\tilde{S}'_3 - \tilde{S}''_2]^a + [\tilde{S}'_3 - \tilde{S}''_3]^a = 4\bar{\sigma}^a \end{aligned} \tag{3}$$

The equivalent stress is the index related to the crystal structure, for body-centered cubic (BCC) material, $a = 6$; for face-centered cubic (FCC) materials, $a = 8$. $\tilde{S}''_{i=1,2,3}$ and $\tilde{S}'_{i=1,2,3}$ is the principal value of the tensor \tilde{S} and \tilde{S}'' , which is obtained by transformation of the stress partial tensor S .

$$\tilde{S}' = C' s = C' T \sigma = L' \sigma \tag{4}$$

$$\tilde{S}'' = C'' s = C'' T \sigma = L'' \sigma \tag{5}$$

$$C' = \begin{pmatrix} 0 & -c_1 & -c_2 & 0 & 0 & 0 \\ -c_3 & 0 & -c_4 & 0 & 0 & 0 \\ -c_5 & -c_6 & 0 & 0 & 0 & 0 \\ 0 & 0 & 0 & c_9 & 0 & 0 \\ 0 & 0 & 0 & 0 & c_8 & 0 \\ 0 & 0 & 0 & 0 & 0 & c_7 \end{pmatrix} \tag{6}$$

$$C'' = \begin{pmatrix} 0 & -c_{10} & -c_{11} & 0 & 0 & 0 \\ -c_{12} & 0 & -c_{13} & 0 & 0 & 0 \\ -c_{14} & -c_{15} & 0 & 0 & 0 & 0 \\ 0 & 0 & 0 & c_{18} & 0 & 0 \\ 0 & 0 & 0 & 0 & c_{17} & 0 \\ 0 & 0 & 0 & 0 & 0 & c_{16} \end{pmatrix} \tag{7}$$

$$T = \frac{1}{3} \begin{pmatrix} 2 & -1 & -1 & 0 & 0 & 0 \\ -1 & 2 & -1 & 0 & 0 & 0 \\ -1 & -1 & 2 & 0 & 0 & 0 \\ 0 & 0 & 0 & 3 & 0 & 0 \\ 0 & 0 & 0 & 0 & 3 & 0 \\ 0 & 0 & 0 & 0 & 0 & 3 \end{pmatrix} \tag{8}$$

Where σ is the Cauchy stress tensor. C' and C'' is a transformation matrix with 18 anisotropic coefficients, which is used to capture the anisotropy of materials and T is the standard transformation tensor that converts σ into S . $C_1 \sim C_{18}$ are 18 anisotropic parameters of Yld2004-18p yield criterion, which can be calibrated by experimental optimization, $C_1 \sim C_6$ and $C_{10} \sim C_{15}$ represent the shear elastic modulus between different axial directions. C_9 and C_{18} , C_8 and C_{17} , C_7 and C_{16} represent the shear elastic modulus around x, y, z axis respectively.

Material parameter identification

The plastic strain ratio, namely the r -value, is a mechanical parameter used to show the plastic tensile properties of metal sheets in different directions and is an important parameter to evaluate the compression forming of metal sheets [24]. According to (determination of the plastic strain ratio of thin plates and strips of metal materials), the plastic strain ratio r is the ratio of the true strain in the width direction of the specimen to the true strain in the thickness direction of the specimen in the uniaxial tensile test, which is expressed as:

$$r = \frac{\epsilon_b}{\epsilon_t} \tag{9}$$

Where ϵ_b is real strain in the width direction, ϵ_t is real strain in the thickness direction. However, in the process of experiment and data processing, the strain in the thickness direction is not easy to measure. According to the principle of volume invariance, by measuring the length of the gauge section, it can be obtained:

$$r = \frac{\epsilon_b}{\epsilon_t} = \frac{\ln \frac{b}{b_0}}{\ln \frac{t}{t_0}} = \frac{\ln \frac{b_0}{b}}{\ln \frac{l_0 b_0}{l b}} \tag{10}$$

Where b_0 is the width of the original gauge section of the sample (mm), b is the width of the gauge section of the sample after stretching (mm), t_0 is the original thickness of the sample (mm), t is the thickness of the sample after stretching (mm), l_0 is the length of the original gauge section of the sample (mm), l is the length of the gauge section of the sample after stretching (mm).

Table 4 The r -value and yield stress ratio obtained from the tensile tests at different orientations

Angle	Yield stress ratio	r -value	Standard deviation
0°	1	0.82117	0.03364
15°	0.9846	0.89411	0.05576
30°	0.9465	0.96235	0.06102
45°	0.9444	1.10352	0.03679
60°	1.0068	0.95764	0.04543
75°	0.9606	0.81176	0.03168
90°	0.9521	0.79764	0.03571

The larger the plastic strain ratio r in the determined direction, the better the fluidity of the plate in the plane direction. Table 4 shows the r value and yield stress ratio obtained by uniaxial tensile test.

MATLAB is used to input the r -value, yield stress ratio and biaxial tensile yield stress ratio of each angle. The yield stress ratio data of the biaxial tensile test are from the literature [25]. The Yld2004-18p yield function is selected to calculate 18 anisotropic parameters for FE simulation. According to the yield criterion, the plane changes of yield stress ratio and r -value are predicted, and the predicted results are compared with the experimental results. The comparison of the theoretical and experimental results of the yield stress ratio and the r -value is shown in Fig. 7a and b, respectively.

It can be seen from Fig. 10a and b that the Yld2004-18p yield function can accurately predict the yield stress ratio and plastic strain ratio r of different orientations along the rolling direction. Voce's hardening law is incorporated into the anisotropic yield function to construct the elastoplastic model.

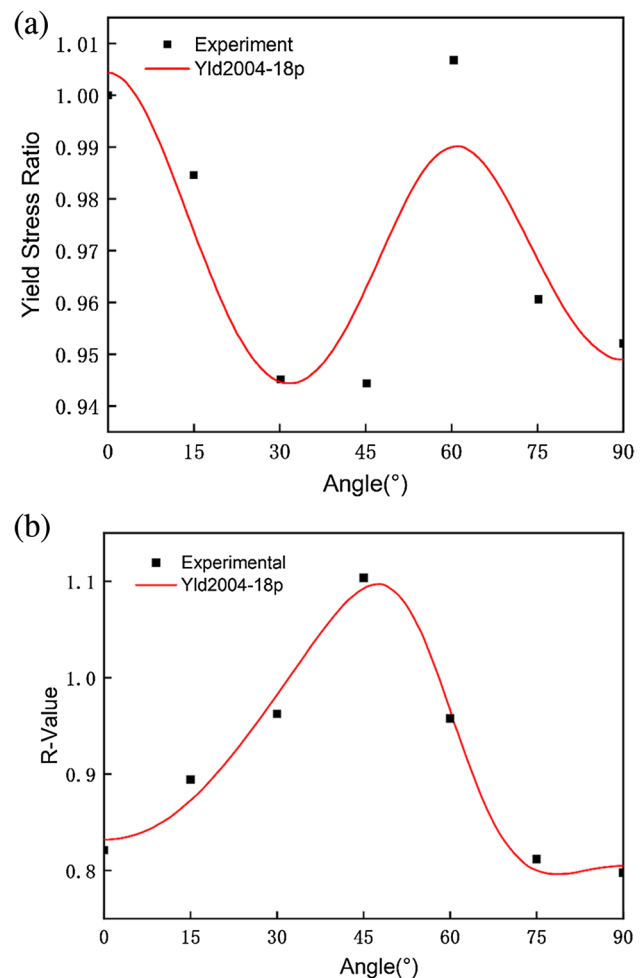
$$\bar{\sigma} = A - B \cdot e^{-C \cdot \bar{\epsilon}^p} \quad (11)$$

Where $\bar{\sigma}$ and $\bar{\epsilon}^p$ are the equivalent stress and the equivalent plastic strain A , B and C are the hardening parameters obtained by fitting the true stress-strain curve obtained by uniaxial tension. In the process of reverse fitting, the stress-strain data measured by the experiment is used as the input data. By adjusting the value of the model parameters, the stress-strain curve calculated by the model is in good agreement with the experimental data. The reverse calibration strategy can improve the accuracy and efficiency of prediction, especially when predicting large deformation and plastic instability [26, 27].

FE modelling of micro-deep drawing

Finite element model

ABAQUS is a powerful FE software for engineering simulation. It can simulate linear and nonlinear problems and can be customized according to user-specific analysis

**Fig. 7** Comparison of theoretical and experimental (a) values of the yield stress ratio, and (b) the r -value

requirements. This paper establishes the deep drawing simulation model of a cylindrical cup based on Abaqus. The whole model is composed of four parts: punch, blank holder, blank and die, as shown in Fig. 8a. The diameter of the punch is 4mm, the diameter of the die is 4.26mm, and the radius of the punch and the die are both 1mm. The blank holder and the die are coupled and fixed, and the displacement of the punch is applied for deep drawing simulation. The binder force is set to 107 N. The whole drawing process is regarded as a quasi-static problem, so the implicit solver ABAQUS/Standard is selected. Because the specimen has geometric axisymmetric characteristics, to improve the calculation efficiency and ensure accuracy, a 1/4 model is used. The punch, die, and blank holder have almost no deformation in the actual stamping process [28], so these three parts are set as analytical rigid shells in the software. The hexahedral shape is selected for the grid division of the sheet metal. Considering the contact between the punch fillet and the sheet metal, it is divided into two regions, as shown

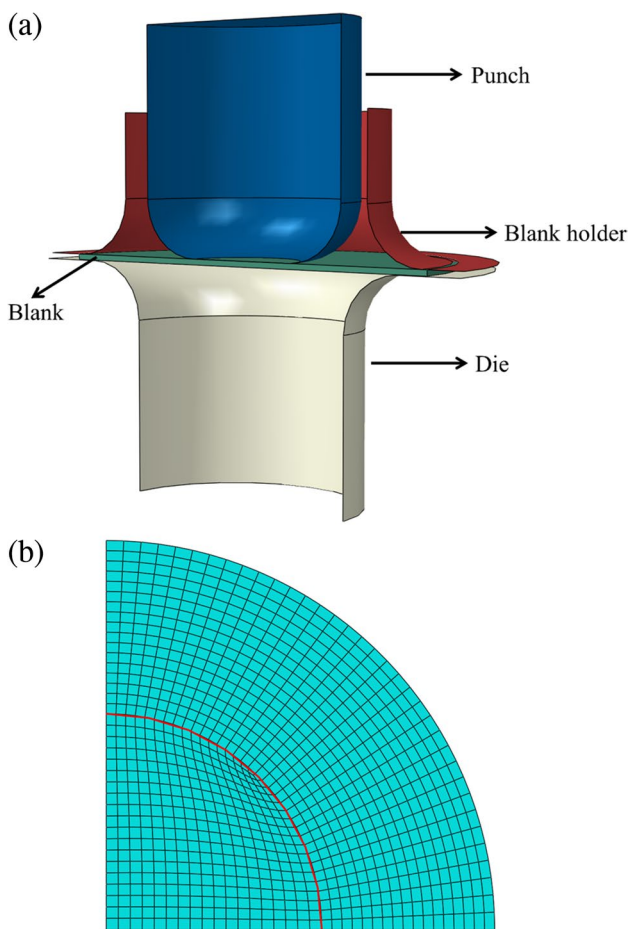


Fig. 8 FE preparation (a) The general FE model, and (b) The mesh of the flat blank for the micro-deep drawing

in Fig. 8b. The quarter of the blank consists of 2808 C3D8R elements and 3960 nodes.

The first pair of contacts is the upper surface of the blank and the punch, the second pair is the contact between the upper surface of the blank and the blank holder, and the third pair is the lower surface of the blank and the die. The contact is defined as the contact between the surface and the surface. The contact property option selects the tangential behavior, and the friction coefficient is set to 0.1.

The simulation is divided into six analysis steps: The first step is to ensure that the gap between the blank and the blank holder and the die is maintained at the level of 0.001 mm, and the contact is carried out by setting the displacement boundary condition. The second step is to remove the displacement boundary condition in the z direction of the blank holder, and to apply the downward

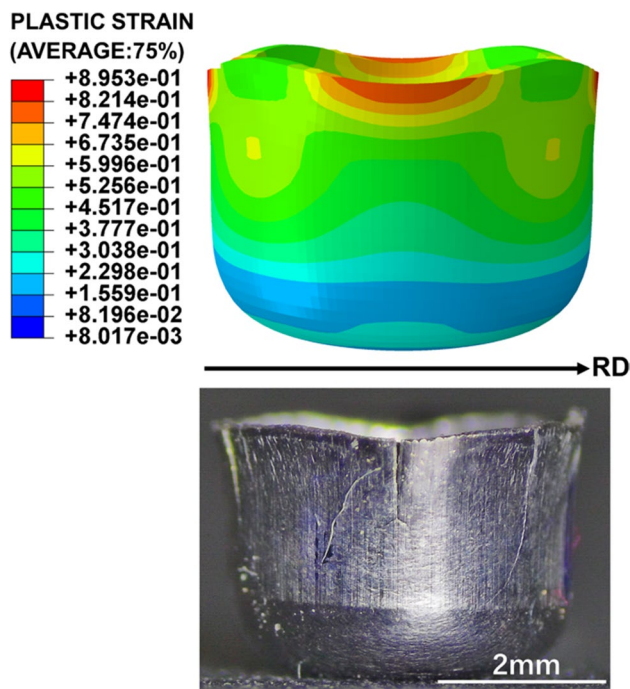


Fig. 9 Comparison between FE predicted and experimentally formed shapes

blank holder force to ensure the solid contact between the blank and the blank holder and the die. The third step: the contact between the blank and the punch is realized by displacement; the fourth step: remove the z-direction displacement boundary condition of the punch, and apply a small negative tension to the blank; the fifth step: further improve the z-direction displacement boundary condition of the punch until all the materials enter the die fillet area; the sixth step: after the blank enters the round corner area of the die, the three-way fixed boundary condition of the blank holder is added, and the punch continues to move down until the forming is completed.4.2 Shape Analysis of Cylindrical Cup.

Taking the deep drawing of cylindrical cup with a sheet thickness of 0.2mm and a punch diameter of 4mm at room temperature as an example, the FE simulation is carried out. The FE simulation results and the cylindrical cup obtained from the experiment are shown in Fig. 9.

It can be clearly observed that there are four ears in the cylindrical cup. The distribution of ears and the fluctuation of ears are consistent. Taking 1/4 cylindrical cups as an example, all of them are at 45° with the rolling direction, and the height of the cylindrical cup reaches the maximum, forming the ear peak.

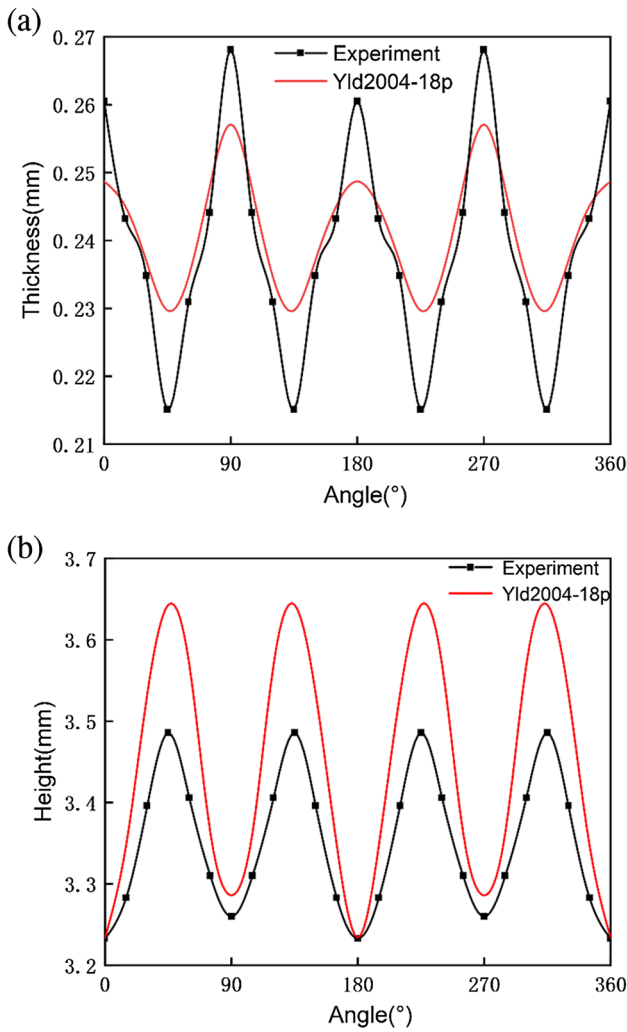


Fig. 10 Comparison between FE predicted and experimentally measured results of (a) the wall thickness; and (b) the height of the MDD formed barrel

Comparison with experiments

The thickness and height of the cylinder wall affect the volume of the material flowing to the height direction of the cylinder wall, so the accuracy of the prediction is very important for the prediction of the ear shape. The thickness and height of the cylinder wall are measured by an industrial camera. When measuring, marking is started from the rolling direction, marking is marked every 15°, and the wall thickness and height corresponding to each degree are measured. The wall thickness and cylinder height of the FE analysis results are compared with the experimental results, as shown in Fig. 10a and b, respectively.

It can be seen from the figure that the wall thickness and cylinder height curves obtained based on the Yld2004-18p yield function are roughly the same as the test curves. It can

be obtained that the FE deep drawing simulation predicts the thickness and height distribution in all directions, which is in good agreement with the test results.

Discussion

Deformation mechanisms of the micro-deep drawing process

In order to study the deformation mechanism of 304 stainless steel in deep drawing and further show the response of the blank in the deep drawing process, the deep drawing test curve of 304 stainless steel cylindrical cup at room temperature is divided into stages, as shown in Fig. 11. Figure 12 is the deformation diagram of the blank from the initial elastic deformation stage to the different stages of plastic forming. The stage division is set to six stages, representing the six deformation states in the Fig. 11. Stage I represents that the punch and the blank begin to contact, and the contact part has elastic deformation. With the downward movement of the punch, the blank began to undergo plastic deformation and plastic expansion in stage II, and the blank began to come into contact with the rounded part of the die, resulting in a larger force required in this stage. Stage III is called the uniform plastic deformation stage, and the blank evenly enters between the punch and die. At stage IV, the blank began to neck circumferentially and was accompanied by thinning. Macroscopically, the thickness of the blank began to decrease in the local area near the corner of the punch. When the blank is about to break away from the blank holder, the drawing force reaches the maximum. Stage V continues to undergo plastic deformation and material neck reduction, but the drawing force decreases rapidly. Although

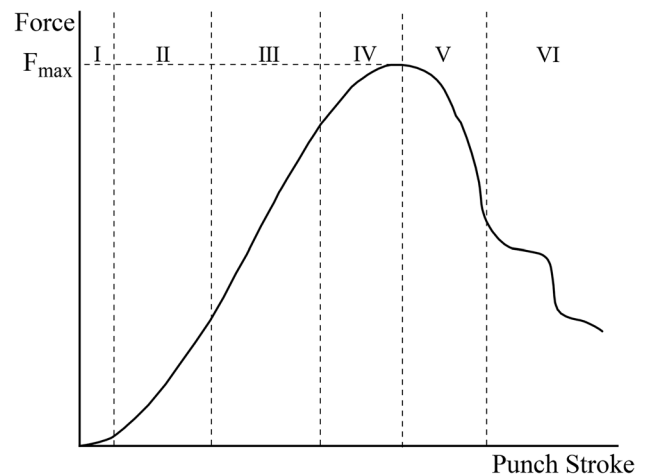


Fig. 11 The schematic diagram of the deep drawing force-punch stroke curve

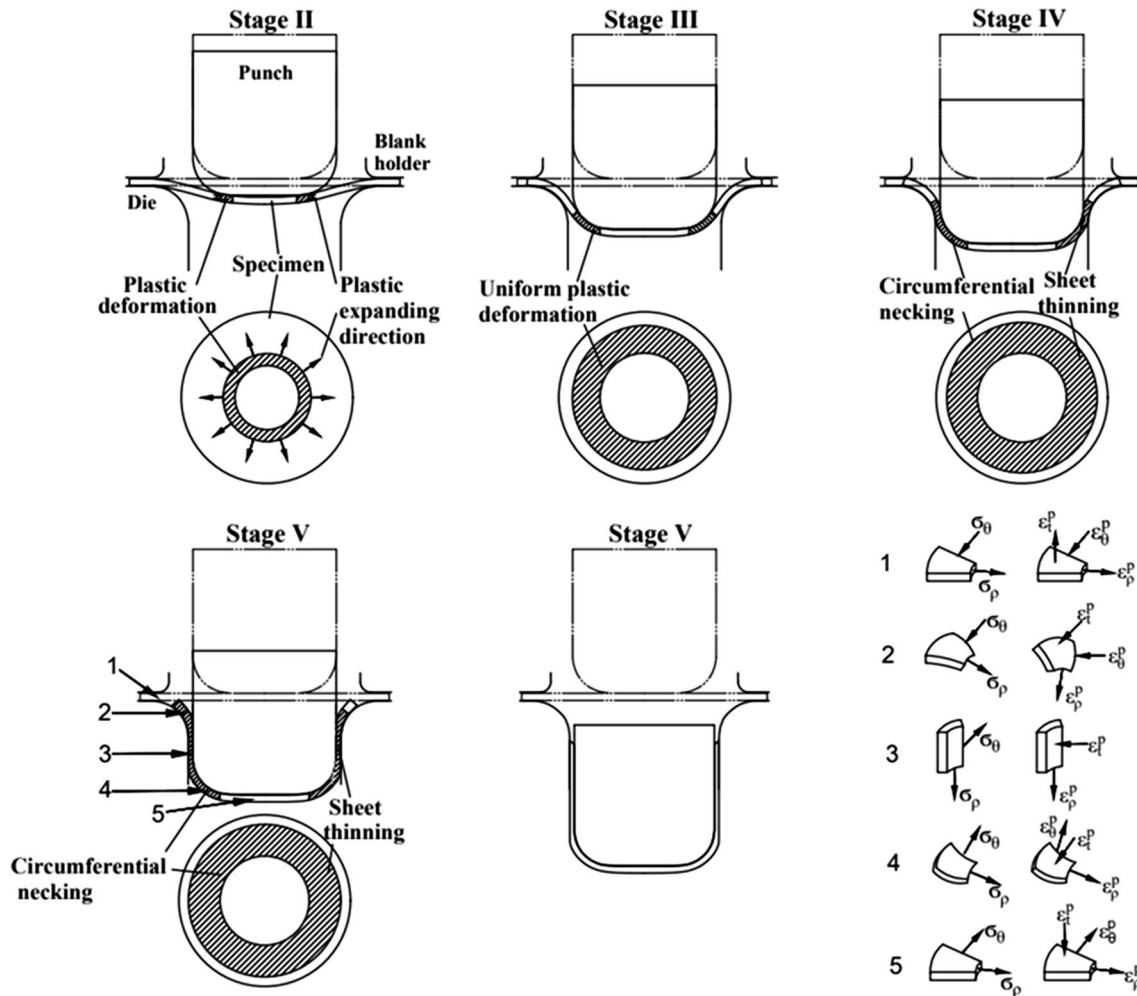


Fig. 12 Schematic diagrams of deformation regimes, deformation mode, and the associated stress states over the complete MDD process

the blank has been separated from the round corner of the die at this time, there are still some blanks in contact with the lower half of the round corner of the die, and the drawing force is reduced at different rates in stage VI. All the blanks enter between the punch and the die, and the deep drawing of the cylindrical cup is completed.

The deformation of the plane flange part of 304 stainless steel cylindrical cup is the largest, which is the main deformation area, and is accompanied by the trend of thickening. The deformation of the inner side of the middle side wall is larger. The outer side of the middle side wall contacts with the die when it is subjected to reverse extrusion pressure, and the deformation is larger [29]. The inner side of the bottom fillet contacts with the punch during the forming process, and the grain deformation accelerates. At this time, the grain size is small. Different degrees of grain refinement occurred in the above parts [30, 31]. The bottom of the cylinder cup is thinner, and the centre belongs to the small deformation area after stamping. There is no deformation but thinning. In

addition, there is almost no plastic deformation at the inner and outer sides of the port, the outside of the bottom rounded corner and the inner and outer sides of the bottom centre, and the grain size remains unchanged.

The effect of anisotropic plasticity

Set in the anisotropic model used, the plastic strain ratio of each angle is set to 1, the 18 anisotropic parameters will be changed to 1 accordingly, and other conditions remain unchanged, which is equivalent to the application of isotropic model simulation of the deep-drawing process, the simulation results are shown in the Fig. 13, and the phenomenon of ears disappeared. The plastic strain ratio of different angles between the blank and the rolling direction is different, so the formed cylindrical cup has ears. That is, the greater the plastic strain ratio r value, the faster the flow rate of the blank plane, and the stronger the deformation ability of the material in the drawing process, so the ear peak will

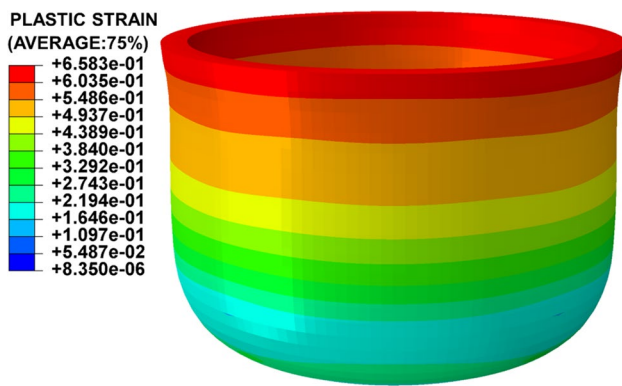


Fig. 13 Simulation result of isotropic model

appear in the direction of the larger r value. According to the principle of constant volume, the higher the height of the ear, the thinner the thickness of the blank will be; on the contrary, a smaller plastic strain ratio will lead to a decrease in the height of the ear and a thickening phenomenon. Therefore, the wall thickness of the ear valley is higher than that of the ear peak.

Plastic anisotropy will lead to different deformation capacity of materials in different directions. In the process of deep drawing, if the plastic deformation ability of the material in some directions is weak, the depth or shape of the forming may be limited, that is, the macroscopic ears phenomenon is formed; Plastic anisotropy may also affect the surface quality of the formed parts. If the plastic deformation ability of the material in some directions is weak, it may lead to wrinkles, cracks or other defects on the surface of the formed part, which is manifested as wrinkling on the cylindrical cup.

Conclusions

The deep drawing and uniaxial tensile tests of 304 stainless steel sheets with different orientations along the rolling direction at room temperature were carried out. In order to explore the influence of anisotropy on the deep drawing of the cylindrical cup, based on the experimental data, the Yld2004-18p yield function was introduced, and Voce's hardening law was combined. The FE simulation of the deep drawing process was carried out, and the wall thickness and height of the cylindrical cup and the distribution of the ears obtained by the FE and the test were compared. The conclusions obtained in this paper are as follows:

- In the forming process of cylindrical cups, the forming quality will be affected by many factors, such as blank thickness and punch diameter. Through the stage division

of the deep drawing experiment, it is found that there are different degrees of deformation in each part after forming: the deformation of the flange area is the largest and accompanied by a thickening trend; the outer side of the middle side wall is subjected to reverse extrusion when it contacts with the die. The punch fillet area as the force transmission area is the transition area between the blank flowing into the punch and die.

- Yld2004-18p, yield function can accurately simulate the earing phenomenon and its distribution of cylindrical cups due to material anisotropy, and the thickness and height of the cylinder wall obtained by simulation are close to the experimental values. The mean absolute error(MAE) of thickness is 0.006974, and the MAE of height is 0.08626.

Acknowledgements The authors are grateful to the Ministry of Science and Technology of the P.R. China (G2021003007L). This work is also supported by the Modern Equipment Manufacturing Collaborative Innovation Center of Southern Hebei New District.

References

1. Persano A, Quaranta F, Taurino A, Siciliano PA, Iannacci J (2020) Thin film encapsulation for RF MEMS in 5G and modern telecommunication systems. *Sensors* 20(7):2133. <https://doi.org/10.3390/s20072133>
2. Tao K, Tang L, Wu J, Lye SW, Chang H, Miao J (2018) Investigation of multimodal electret-based MEMS energy harvester with impact-induced nonlinearity. *J Microelectromech Syst* 27:276–88. <https://doi.org/10.1109/JMEMS.2018.2792686>
3. Arbabi E, Arbabi A, Kamali SM, Horie Y, Faraji-Dana MS, Faraon A (2018) MEMS-tunable dielectric metasurface lens. *Nat Commun* 9(1):812. <https://doi.org/10.1038/s41467-018-03155-6>
4. Mallik S, Chowdhury D, Chhtopadhyay M (2019) Development and performance analysis of a low-cost MEMS microphone-based hearing aid with three different audio amplifiers. *Innov Syst Softw Eng* 15:17–25. <https://doi.org/10.1007/s11334-019-00325-7>
5. Xu Q, Li X, Chan CY (2018) Enhancing localization accuracy of MEMS-INS/GPS/in-vehicle sensors integration during GPS outages. *Ieee T Instrum Meas* 67(8):1966–1978. <https://doi.org/10.1109/TIM.2018.2805231>
6. Shimizu T, Ogawa M, Yang M, Manabe K (2014) Plastic anisotropy of ultra-thin rolled phosphor bronze foils and its thickness strain evolution in micro-deep drawing. *Mater Des* 56:604–612. <https://doi.org/10.1016/j.matdes.2013.11.048>
7. Tang W, Huang S, Li D, Peng Y (2015) Mechanical anisotropy and deep drawing behaviours of AZ31 magnesium alloy sheets produced by unidirectional and cross rolling. *J Mater Process Technol* 215:320–326. <https://doi.org/10.1016/j.jmatprotec.2014.08.020>
8. Demin VA, Larin SN, Riskin RV, Rizkova AA (2018) Study the influence of anisotropy on the drawing cylindrical part. *CIS Iron Steel Rev* 16:25–28. <https://doi.org/10.17580/cisisr.2018.02.05>
9. Yoon JH, Cazacu O, Yoon JW, Dick RE (2010) Earing predictions for strongly textured aluminum sheets. *Int J Mech Sci* 52(12):1563–1578. <https://doi.org/10.1016/j.ijmecsci.2010.07.005>
10. Plunkett B, Cazacu O, Barlat F (2008) Orthotropic yield criteria for description of the anisotropy in tension and compression of

- sheet metals. *Int J Plasticity* 24(5):847–866. <https://doi.org/10.1016/j.jiplas.2007.07.013>
11. Banabic D, Barlat F, Cazacu O, Kuwabara T (2020) Advances in anisotropy of plastic behaviour and formability of sheet metals. *Int. J. Mater* 13:749–787. <https://doi.org/10.1007/s12289-020-01580-x>
 12. Habraken AM, Aksen TA, Alves JL (2022) Analysis of ESA-FORM 2021 cup drawing benchmark of an Al alloy, critical factors for accuracy and efficiency of FE simulations. *Int. J. Mater* 15(5):61. <https://doi.org/10.1007/s12289-022-01672-w>
 13. Lou Y, Zhang S, Yoon JW (2019) A reduced Yld 2004 function for modeling of anisotropic plastic deformation of metals under triaxial loading. *Int J Mech Sci* 161:105027. <https://doi.org/10.1016/j.jmeosci.2019.105027>
 14. Rong H, Ying L, Hu P, Hou W (2021) Characterization on the thermal anisotropic behaviors of high strength AA7075 alloy with the Yld 2004–18p yield function. *J Alloy Compd* 877:159955. <https://doi.org/10.1016/j.jallcom.2021.159955>
 15. Neto DM, Oliveira MC, Alves JL, Menezes LF (2014) Influence of the plastic anisotropy modelling in the reverse deep drawing process simulation. *Mater Des* 60:368–379. <https://doi.org/10.1016/j.matdes.2014.04.008>
 16. Chai L, Luan B, Xiao D, Zhang M, Murty KL, Liu Q (2015) Microstructural and textural evolution of commercially pure Zr sheet rolled at room and liquid nitrogen temperatures. *Mater Des* 85:296–308. <https://doi.org/10.1016/j.matdes.2015.06.088>
 17. He W, Li F, Zhang H, Chen H, Guo H (2019) The influence of cold rolling deformation on tensile properties and microstructures of Mn18Cr18 N austenitic stainless steel. *Mat Sci Eng* 764:138245. <https://doi.org/10.1016/j.msea.2019.138245>
 18. Liu H, Wang Y, Li B, Ma X, Wu R, Hou L, Zhang J, Zhang M (2019) Effect of cryogenic rolling process on microstructure and mechanical properties of Mg-14Li-1Al alloy. *Mater Charact* 157:109903. <https://doi.org/10.1016/j.matchar.2019.109903>
 19. Basak S, Panda SK, Lee MG (2020) Formability and fracture in deep drawing sheet metals: Extended studies for pre-strained anisotropic thin sheets. *Int J Mech Sci* 170:105346. <https://doi.org/10.1016/j.jmeosci.2019.105346>
 20. Hu P, Liu YQ, Wang JC (2001) Numerical study of the flange earring of deep-drawing sheets with stronger anisotropy. *Int J Mech Sci* 43(1):279–296. [https://doi.org/10.1016/S0020-7403\(99\)00119-8](https://doi.org/10.1016/S0020-7403(99)00119-8)
 21. Othmen KB, Sai K, Manach PY, Elleuch K (2019) Reverse deep drawing process: material anisotropy and work-hardening effects. *P I Mech Eng L-J Mat* 233(4):699–713. <https://doi.org/10.1177/146442071770195>
 22. Tiwari P R, Rathore A, Bodkhe M G(2022) Factors affecting the deep drawing process–A review. *Mater Today: Proc* 56:2902–2908. <https://doi.org/10.1016/j.matpr.2021.10.189>
 23. Bruschi S, Altan T, Banabic D, Bariani PF, Brosius A, Cao J, Ghiotti A, Khraisheh M, Merklein M, Tekkaya AE (2014) Testing and modelling of material behaviour and formability in sheet metal forming. *Cirp Ann-Manuf Techn* 63(2):727–749. <https://doi.org/10.1016/j.cirp.2014.05.005>
 24. Nachbagger K (2014) State of the art of ANCF elements regarding geometric description, interpolation strategies, definition of elastic forces, validation and the locking phenomenon in comparison with proposed beam finite elements. *Arch Comput Method Eng* 21(3):293–319. <https://doi.org/10.1007/s11831-014-9117-9>
 25. Yadav A D (2008) Process analysis and design in stamping and sheet hydroforming. PhD dissertation The Ohio State University:175
 26. Tuninetti V, Oñate A, Valenzuela M (2023) Characterization approaches affect asymmetric load predictions of hexagonal close-packed alloy. *J. Mater. Res. Technol.* 26:5028–5036. <https://doi.org/10.1016/j.jmrt.2023.08.255>
 27. Sun W, Yue Z, Wen Z, Li M (2023) An overview on material parameter inverse and its application to miniaturized testing at elevated temperature. *J. Mater. Res. Technol.* 22:3132–3145. <https://doi.org/10.1016/j.jmrt.2022.12.159>
 28. Bouchaâla K, Ghanameh MF, Faqir M, Mada M, Essadiqi E (2021) Numerical investigation of the effect of punch corner radius and die shoulder radius on the flange earring for AA1050 and AA1100 aluminum alloys in cylindrical deep drawing process. *Heliyon* 7(4). <https://doi.org/10.1016/j.heliyon.2021.e06662>
 29. Cai G, Yang J, Yuan Y, Yang X, Lang L, Alexandrov S (2020) Mechanics analysis of aluminum alloy cylindrical cup during warm sheet hydromechanical deep drawing. *Int. J. Mech. Sci* 174:105556. <https://doi.org/10.1016/j.jmeosci.2020.105556>
 30. Zheng G, Li X, Chang Y, Wang C, Dong H (2018) A comparative study on formability of the third-generation automotive medium-Mn steel and 22MnB5 steel. *J Mater Eng Perform* 27:530–540. <https://doi.org/10.1007/s11665-018-3183-3>
 31. Narayanasamy R, Narayanan CS (2008) Forming, fracture and wrinkling limit diagram for if steel sheets of different thickness. *Mater Des* 29(7):1467–1475. <https://doi.org/10.1016/j.matdes.2006.09.017>

Publisher's Note Springer Nature remains neutral with regard to jurisdictional claims in published maps and institutional affiliations.

Springer Nature or its licensor (e.g. a society or other partner) holds exclusive rights to this article under a publishing agreement with the author(s) or other rightsholder(s); author self-archiving of the accepted manuscript version of this article is solely governed by the terms of such publishing agreement and applicable law.